Magnitude Thresholds and Spatial Footprints of Damage from Induced Earthquakes

Bridger W. Baird,[a] M.EERI, Abbie B. Liel,[b] M.EERI, and Robert E. Chase [c] M.EERI

The rise in the number of anthropogenic small to moderate magnitude earthquakes in the central United States raises questions about the damageability of the built environment in such events. This study examines the performance of modern light-frame wood buildings, including single, multi-family and commercial construction, in earthquakes with moment magnitude of 3 to 6, using dynamic analysis of buildings models subjected to ground motions recorded in past induced events in North America. We focus on first onset of damage, e.g., wallboard or wallpaper cracking, nails popping out. The results show that earthquakes with magnitude less than 4-4.25 are unlikely to cause damage to modern construction. However, moderate magnitude events can cause damage over a wide geographic area (more than 30 miles from the earthquake epicenter, or 40 or more miles from a wastewater injection well). These results can be used to suggest setback distances between injection wells and certain neighborhoods or facilities, and magnitude thresholds for post-earthquake inspections.

INTRODUCTION

OVERVIEW

The U.S. states of Oklahoma (OK), Texas, and Kansas have been experiencing elevated numbers of small- to moderate-magnitude earthquakes (*e.g.,* Ellsworth et al. 2015; Petersen et al. 2018). Prior to 2009, historical earthquake rates for OK averaged about two earthquakes with moment magnitude (**M**) > 3.0 per year. Recently, these rates have been as high as 700 events with **M** > 3.0 in a year and, in 2018, the state experienced about 200 such earthquakes

[a] Civil, Environmental, and Architectural Engineering, University of Colorado, Boulder, 1111 Engineering Dr., Boulder, CO 80309; Email: bridger.baird@colorado.edu (B. W. B.)
[b] Civil, Environmental, and Architectural Engineering, University of Colorado, Boulder, 1111 Engineering Dr., Boulder, CO 80309; Email: abbie.liel@colorado.edu (A. B. L.)
[c] Exponent, 1331 17th Street Suite 515, Denver, CO 80202; Email: robert.chase@colorado.edu (R. E. C.)

(OGS, 2018). This seismicity is largely the result of the deep injection of large quantities of wastewater from oil and gas development and production activities (*e.g.,* Rubinstein and Mahani 2015; Weingarten et al. 2015).

These earthquakes have caused damage to the region's built infrastructure. For example, after the 2016 **M** 5.0 Cushing, OK earthquake, documented damage included: cracking in mortar joints, spalling or partial collapse of brick veneer, racking of structures, damage to brick chimneys, and water main bursts (Barba-Sevilla et al. 2018). Much of the damage from the Cushing earthquake was cosmetic or nonstructural and occurred in older light-frame wood buildings with a masonry brick veneer. Similar patterns of damage have been experienced in other recent OK earthquakes (*e.g.,* Taylor et al. 2018), and observed in analytical studies (Chase et al. 2019).

This increase in earthquake activities corresponds to elevated seismic hazard in the region (*e.g.,* Petersen et al. 2016, 2017, 2018) which, in turn, corresponds to elevated risk to buildings and infrastructure in the region. Liu et al. (2019) showed significant increases in risks of building performance that endangers life safety compared to that due to non-induced earthquakes alone; the degree to which risk was elevated was found to vary from a few times to more than 100 times, depending on location, building period (or, building height), and the type of risk of interest.

Mitigation strategies aim to reduce the risk from induced seismicity by (Bommer et al. 2015): reducing seismic hazard, making the building and infrastructure stock more robust (*i.e.,* reducing fragility), or avoiding or reducing exposure of communities or certain facilities to these events. In the context of mitigating risk from *tectonic* earthquakes, because we cannot control the tectonic seismic hazard, efforts generally aim to improve seismic performance of structures, reducing fragility. In contrast, because induced seismicity is anthropogenic, risk mitigation strategies have generally focused on seismic hazard, aiming to decrease the expected

frequency or magnitude of induced events (Bommer et al. 2015). Although building strengthening is a component of induced seismicity risk mitigation strategies in the Netherlands (van Elk et al. 2019), the wastewater injection that causes these events in and around OK is highly volatile depending on global oil and gas markets and other factors, and neither building code changes nor retrofits of existing buildings appear to be feasible on a large scale.

Efforts to mitigate hazard and risk are often guided by so-called 'Traffic Light Systems', which react to certain induced events to by changing operations (GWPC/IOGCC 2017, Majer et al. 2012). These systems generally define red, amber and green lights. The red zone has been defined as "the level of ground shaking at which damage to building in the area is expected to set in" (Majer et al. 2012), though different systems have different principles to define this zone. For example, Ohio requires operators to suspend operation if an event larger than magnitude[1] 1.0 is observed near the site to investigate the cause (Wong et al. 2015). Likewise, regulators in the U.K. halt hydraulic fracturing operations if earthquakes with magnitude 0.5 or above occur (BEIS 2013). In both of these cases, it has been argued that the threshold for stopping operations (the "red light" threshold) is overly conservative, potentially unnecessarily alarming the public. OK has a Traffic Light System around suspect wells, which are those that are near an earthquake swarm (about 350 of 900 Class II wells in the state) (Wong et al. 2015); suspect wells are operated under a "yellow light" condition, requiring additional seismic monitoring and reporting, and a well-specific magnitude threshold between magnitude 1.8 and 3.7 is defined, which will change operations if an earthquake is deemed to be associated with a particular well.

In the context of U.S. injection-induced seismicity, efforts to reduce seismic hazard generally have modified injection operations, for example, by reducing injection volumes or

[1] Note that these systems use different definitions of earthquake magnitude and some regulators may not even identify their definition of magnitude, so we are using the generic term "magnitude" in this paragraph.

eliminating connection between the disposal interval and the basement (Langenbruch et al. 2018, Brown et al. 2017). In general, reducing injection volumes does reduce earthquake rates (e.g., Langenbruch and Zoback 2016), though large earthquakes may still occur (Bommer et al. 2015, Majer et al. 2007; Wong et al. 2015), and there is little science to support the choice of any particular magnitude threshold triggering such a change. Several authors have argued that these systems could be improved by linking thresholds to ground shaking levels, rather than magnitude, *e.g.* Majer et al. 2012, Wong et al. (2015), Walters et al. (2015).

Recognizing that induced earthquakes tend to occur in close proximity to injection operations, exposure may be reduced by locating wells sufficiently far from critical infrastructure and/or communities (Bommer et al. 2015, Atkinson 2017). Goebel and Brodksy (2018) found that, for some sites, particularly where injection is above the crystalline basement, injection wells can cause earthquakes at distances further than 6 miles (10 km) away from the well; this appears to be the case in at least some parts of OK (Yeck et al. 2016). However, for many wells, these distances may be much shorter (Goebel and Brodsky 2018). To reduce exposure to potential events, regulators can impose what are known as "exclusion zones", or setbacks from certain buildings or infrastructure, such as critical facilities, where injection operations are not allowed. For example, in response to induced seismicity in Alberta and British Columbia from hydraulic fracturing, Atkinson (2017) argues that an exclusion zone of ~3 miles (5 km) in radius should be required around critical facilities (*i.e.,* hospitals, important bridges, etc.). However, Atkinson (2017) notes that the area of potential impact around a wastewater injection well is larger than for hydraulic fracturing wells, and suggests a radius on the order of ~6 miles (10 km) for injection wells. Mutz (2019)'s review of regulations in seven western states found that Ohio does not allow Class II underground injection wells within designated distances from various categories of buildings and transportation infrastructure; the relevant setback distances are 50 to 100 ft. Likewise, Colorado allows well permit denial if the

Colorado Oil and Gas Conservation Commission's Director has "reasonable cause to believe that the proposed disposal well could result in a significant adverse impact on the environment or public health, safety and welfare." Other states have setbacks related to proximity to faults, but not proximity to infrastructure (Mutz, 2019).

SCOPE

The goal of this study is to define magnitude thresholds and spatial footprints that are associated with building damage in injection-induced earthquakes. We focus on modern light-frame wood structures, as light-frame wood buildings are the primary building type in OK and elsewhere in the U.S. (van de Lindt and Dao 2009), and similar buildings have sustained damage in past events (*e.g.,* Taylor et al. 2016). First, we dynamically analyze the seismic response of three light-frame wood buildings in more than 50 earthquake scenarios. Three-dimensional (3D) nonlinear models of the buildings are subjected to recorded ground motions from induced earthquakes, and the structural responses are recorded. The first instance of damage, physically manifested by screws popping out, minor cracking of wallboard, and warping or cracking of wallpaper in light-frame wood shear walls, is identified in the responses using damage fragility curves for common components in these buildings. These results quantify the probability of damage for these buildings in a given earthquake scenario, and the spatial footprint or extent of the damage, with the goal of informing mitigation efforts and post-earthquake inspection procedures.

METHODS

EARTHQUAKE SCENARIOS AND GROUND MOTIONS

We begin by defining Earthquake Scenarios of interest, which cover a wide range of possible earthquakes in Oklahoma, with magnitudes, **M,** ranging from 3.0 to 6.0, and hypocentral distances, *i.e.* distances between the focus or hypocenter and a site of interest, ranging from 1.9 to 161.6 miles (3 to 260 km), as shown in Figure 1. We selected a **M** 3.0

event as the minimum because it is on the low end of a potentially damaging earthquake; we selected a **M** 6.0 event because it is slightly larger than the Pawnee **M** 5.8 event, the largest earthquake to date in Oklahoma. In terms of distances, we chose a 1.9 mile (3 km) hypocentral distance to represent an event with a very shallow focal depth, occurring directly underneath the structure. Longer distances are considered for higher magnitudes because they have more damage potential at farther distances. These choices are supported by the deaggregation of the USGS one-year hazard forecasts for Pawnee (Petersen et al. 2018), which suggests that **M** < 6 and **R** ~ 3 – 20 miles (~5 – 35 km) dominate the hazard for shaking intensities with annual frequencies of exceedance > 0.002 (Shumway 2019).

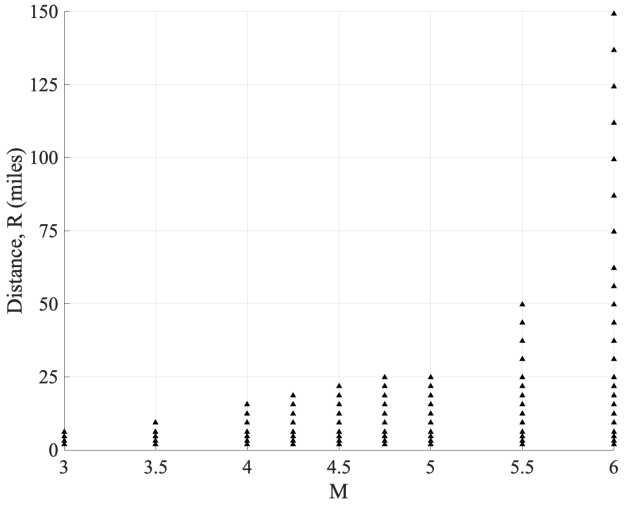

Figure 1. Earthquake Scenarios considered, defined in terms of moment magnitude, **M**, and hypocentral distance, **R**. Each point on the graph represents one of the Earthquake Scenarios.

We use recorded ground motions from induced earthquakes in North America to represent the Earthquake Scenarios for dynamic analysis. These ground motions are from the Assatourians and Atkinson (2018) database of processed induced strong-motions. This database has 68 3-component sets of ground motions. The ground motions were recorded between 2010 to 2016, with **M** > 4.0, and **R** < 31.1 miles (50 km), as shown in Figure 2.

We next select and scale the records to match the intensity and frequency content, and variability therein, of each Earthquake Scenario. To do so, a target spectrum is defined for each

Scenario. The target spectra are produced by the NAA-18 (Novakovic et al. 2018) ground motion prediction equation (GMPE), which has been empirically-calibrated to induced motions in Oklahoma. This GMPE is based on over 7000 ground motion recordings from the Oklahoma region, including approximately 190 events of magnitude 3.5 – 5.8 and hypocentral distances between 2 and 500 km; most of the events have been caused by wastewater injection. NAA-18 takes as input the structure's period, **R**, **M**, rupture depth, and site conditions, *i.e.,* V_{s30}, and produces probabilistic estimates of spectral acceleration. Spectral acceleration is defined by the geometric mean of the two horizontal components. We selected the NAA-18 GMPE because it is based on a large number of recorded ground motions from the region of interest; a number of studies have shown the importance of selecting ground motions and GMPEs specifically for induced earthquakes and the tectonic environment in Oklahoma (*e.g.,* Chase 2018; Moschetti et al. 2019; Atkinson et al. 2018). In particular, the characteristic shallow focal depth of induced events makes near distance scaling particularly important (Atkinson et al. 2018; Zalachoris and Rathje 2019). However, a limitation is that, due to the scarcity of records, there are few records used in the GMPE development that are both at the upper end of the magnitude range and the lower end of the distance range, *i.e.* the range where damage is most likely. Nevertheless, the NAA-18 GMPE produces similar estimates of spectral acceleration values to Zalachoris and Rathje (2019).

To define the target spectrum for a given Earthquake Scenario using the NAA-18 GMPE, **M** and **R** are defined by the Earthquake Scenario of interest. We take the focal depth as 3.1 miles (5 km) for most of the Earthquake Scenarios (excluding Scenarios with **R** of 1.9 miles); this depth was selected to represent typical depth for induced events in Oklahoma (USGS 2019). For events with **R** of 1.9 miles (3 km), the earthquake is assumed to occur directly underneath the structure. We assume a site class C V_{s30} value of 1476 ft/s (450 m/s) to represent soil conditions present in most of Oklahoma (Yong et al. 2016).

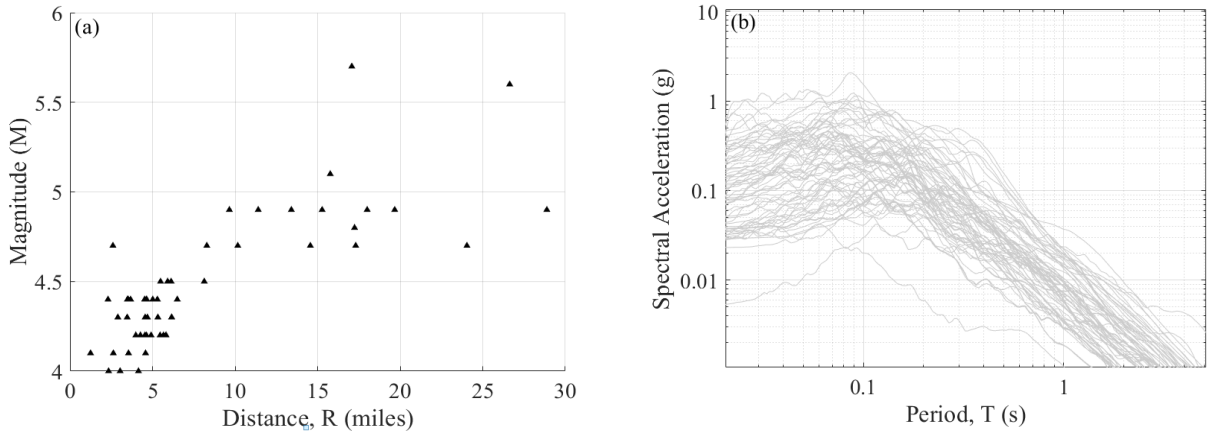

Figure 2. Earthquake and ground motion characteristics for the 68 induced motions collected by Assatorians and Atkinson (2018), showing (a) magnitude and distance distribution and (b) as recorded geomean acceleration response spectra of horizontal components.

We next select a subset of ground motions from the database and define a set of scaling factors to represent the target spectrum. For this purpose, we adopt the ground motion selection and scaling algorithm from Baker and Lee (2018) to select motions that match the target spectra for a given Earthquake Scenario, in terms of both median and standard deviation. Matching the variability is important to represent the variability of structural response for a Scenario, even when the structural response is linear (*e.g.,* Lin et al. 2013). Based on the defined target response spectrum, the ground motion selection algorithm statistically simulates response spectra to match the target spectrum. For each simulated spectrum, a ground motion from the Assatourians and Atkinson (2018) database is selected and linearly scaled to match the statistically simulated spectra. Subsequently, an optimization process that seeks to replace one ground motion at a time to improve the match with the target spectrum based on the error between the target and recorded spectra (Baker and Lee 2018). We aim to match the target spectrum within a range of ~0.2T to 2T, where T is fundamental period of the building, to capture the important range of linear (including higher modes) and nonlinear response. We placed no minimum or maximum limit on the scale factors, and select 25 motions and scale factors for each target spectrum. All calculations are done with geomean spectral accelerations.

Figure 3a provides an example of the ground motions selected to match the target for a **M** 4.5 and **R** 4.7 miles (7.5 km) Scenario. Although, in general, the records matched the target spectra well, the fit was worse at higher magnitudes (Figure 3b), which is a function of the smaller number of records from higher magnitude events available in the Assatourians and Atkinson (2018) database (and in general for OK). We searched for higher magnitude tectonic earthquakes to supplement the database, but ultimately did not include them due to differences in the regional tectonic environment between the available induced and tectonic motions, which have been shown to have an impact on structural response (Chase 2018). The spectra in Figure 3 peak at periods of approximately 0.1 seconds, as expected for induced and other small- to moderate-magnitude events that have peaked, high frequency content.

Ground motions were applied as recorded to 3D building models, with the East-West component in the database applied to the East-West axis of the buildings. More details of the building models are provided below.

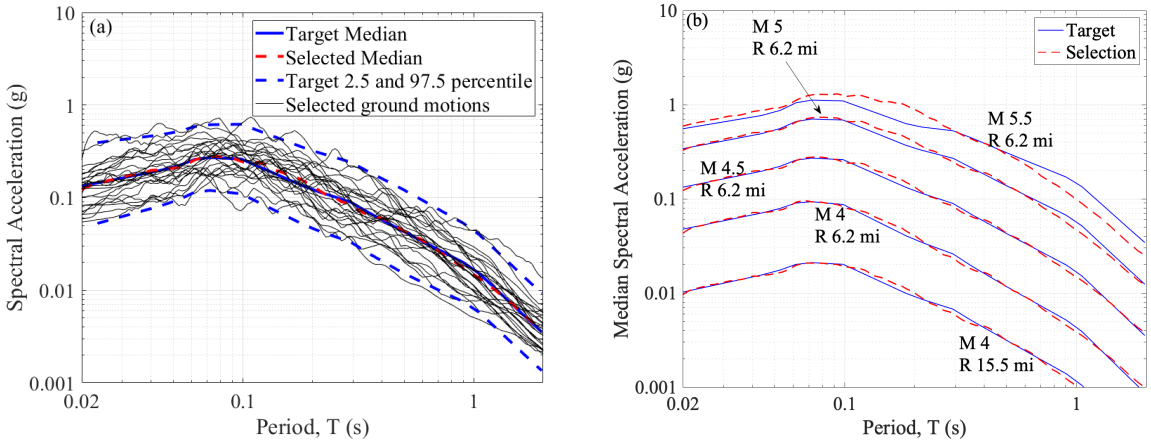

Figure 3. Selected and scaled ground motion records, showing (a) the target spectrum for the **M** 4.5 and **R** of 4.7 miles (7.5 km) Scenario, and the selected motions, and (b) target and selected median spectra comparison for multiple Scenarios.

BUILDING ARCHETYPES

Building Designs

We designed the buildings in this study for Pawnee, OK, which is in seismic design category (SDC) B, with a S_{DS} of 0.139 g for site class C (ASCE 2017). We chose Pawnee to

represent a typical OK location, with relatively small seismic design forces. The three buildings considered in this study were originally designed for "moderate seismicity" according to ASCE 7-10 (ASCE 2010) as part of the ATC 116 project (ATC 2020), for which they were developed and reviewed by practicing professional engineers (see also Ziaei Ghehnavieh 2017). We redesigned for the lower seismicity conditions of Pawnee compared the "moderate seismicity" levels used in the original design. We carried out this design according to ASCE 7-16 (ASCE 2017), using the same wall layouts as the original designs. In this redesign, the shear wall material was changed *(e.g.,* changed from oriented strand board or OSB, to gypsum wall board), the wall lengths decreased, and the nail spacing increased. We confirmed that the SDC B seismic forces controlled over wind for these buildings in Pawnee. Wood (OSB or gypsum) shear wall elements comprise the sole lateral force resisting system in the buildings.

The multi-family building accommodates four two-story 24 ft (7.3 m) by 48 ft (14.6 m) townhomes on a 48 ft (14.6 m) by 96 ft (29.3 m) foundation with a gable roof, as shown in Figure 4. Shear walls are located on the building's exterior and between-unit interior partition walls; these walls are framed with Douglas Fir lumber 2x4s. The exterior face of the exterior wall is clad in a fiber cement (James Hardie) siding over OSB, which is commonly used in OK (Authentic Custom Homes, 2018). The interior face of the exterior walls has 0.5 in (1.3 cm) gypsum wallboard. Additionally, the interior walls and party walls are clad with 0.5 in (1.3 cm) gypsum wallboard in all locations. The floorplan in Figure 4 also shows the location of nonstructural partitions; these partitions are not considered in the design of the building, but are represented in the model and contribute to the seismic resistance of the building. The foundation is a 4 in (10.2 cm) slab on grade. Around the exterior perimeter of the building and underneath the interior load bearing walls, there are reinforced grade beams with footings integrated into the slab on grade. For more details, refer to Baird (2019).

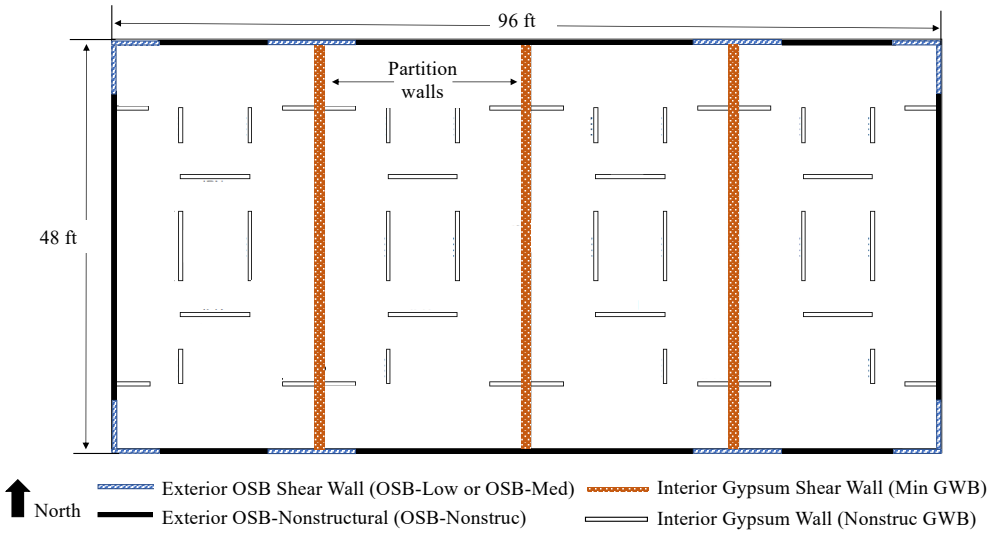

Figure 4. Plan view of the first story of the multi-family building, showing shear and bearing wall layout (modified from ATC 116, 2020). OSB is oriented strand board; GWB is gypsum wall board. Nail and framing details for the wall types listed are provided in Baird (2019) and Ziaei Ghehnavieh (2017).

The two-story commercial building has a 48 ft (14.6 m) by 96 ft (29.3 m) footprint with a flat roof (Figure 5). The walls, framing, siding, and foundation are similar to the multi-family building. However, the commercial building has a 1.5 in (3.8 cm) concrete topping on the floor, which increases the seismic weight of the building. In the interior of the building, the floor and roof trusses are supported by 3 interior steel girders. The interior steel girders are spaced at 24 ft (7.3 m) on center and run parallel to the short wall supported by steel posts. These steel posts do not contribute to the building's seismic resistance. The second-story has some nonstructural partition walls, which represents the division of the building into separate office spaces.

The two-story single-family building has a footprint of 32 ft (9.8 m) by 48 ft (14.6 m) and a gable roof; Figure 6 provides a plan view. The designed shear walls include the exterior walls of the building, as well as the interior gravity load bearing walls. Wall, framing, siding and foundation details are similar to the other buildings.

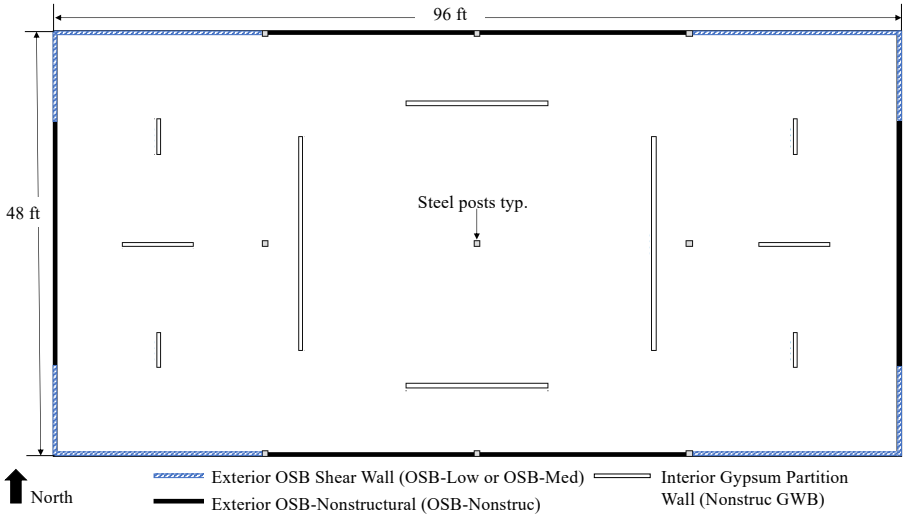

Figure 5. Plan view of the commercial building, showing shear and bearing wall layout (modified from ATC 116, 2020). Nail and framing details for the wall types listed are provided in Baird (2019).

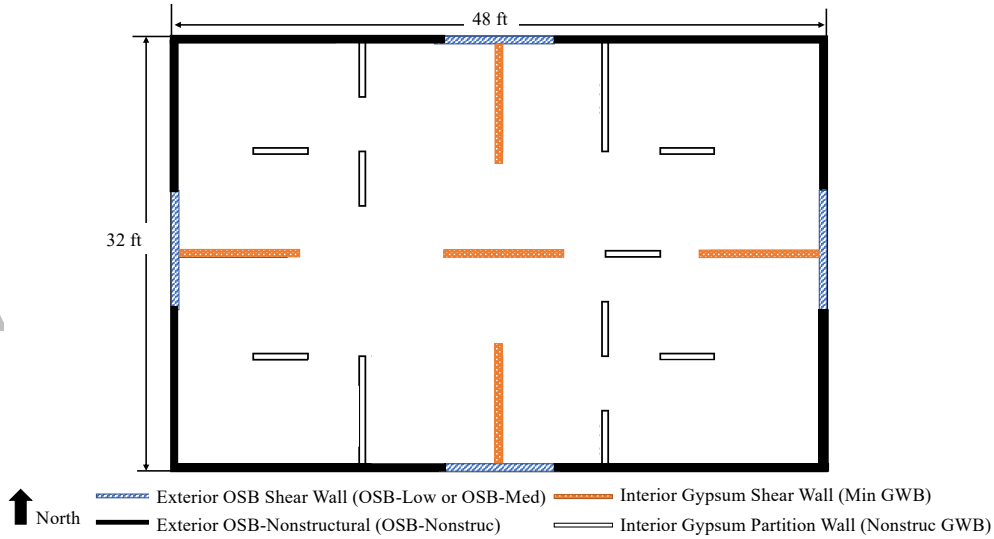

Figure 6. Plan view of the single-family building, showing shear and bearing wall layout (modified from ATC 116, 2020). Nail and framing details for the wall types listed are provided in Baird (2019).

Building Modeling

All three of the buildings in this study are modeled using Timber3D, which is a MATLAB-based analysis software intended for modeling the inelastic dynamic seismic response of short period light-frame wood buildings, developed by Pang and Shirazi (2013). The software is formulated to capture the seismic response of the buildings up to large horizontal and vertical displacements and incipient collapse based on corotational formulation and large displacement theory (Pang and Shirazi 2013). It implements a computationally-efficient version of the finite element methodology with nodal condensation. The approach has been validated by comparing

the model results to experimental tests for various wood shear wall components (Pang and Shirazi 2013); this calibration focused on stiffness, peak strength and deformation capacity. All of the models used in this study were adapted from those developed in ATC 116, and provided to us by Ziaei Ghehnavieh (2017).

Material nonlinear behavior of the three building archetypes is modeled only in the shear wall elements: exterior walls, interior partition walls (structural and nonstructural), and the exterior siding (finishes). The Modified Stewart (MSTEW) model (Folz and Filiatrault 2001) defines the backbone and hysteretic properties of the walls, illustrated in Figure 7. A modification to the MSTEW hysteresis developed by Ziaei Ghehnavieh (2017) applies to all wall elements in these models except for exterior siding. The modification fits an "S" curve to the post peak response of the shear walls to more accurately capture nonlinear strength decay of the shear walls and the residual strength of the shear walls after large displacements. Ziaei Ghehnavieh (2017) calibrated the hysteretic model parameters for the wall types of interest to experimental results. For the exterior walls of the building models, the structural shear walls are assigned to the same location as the siding, such that the exterior wall response represents the composite response of the two components.

Floor diaphragms are modeled using elastic beam elements, but these elements are very stiff, which is consistent with Ziaei Ghehnavieh (2017). Due to the rigid frame-to-frame link elements representing hold downs and anchor bolts, the building models have what amounts to a fixed base. The most important source of damping is the hysteresis response in the nonlinear nonstructural and structural elements (Figure 7). Additionally, we apply 1% Rayleigh damping anchored at periods defining the fundamental modes in both orthogonal directions of the structure to represent a modest amount of linear elastic damping, while also avoiding overdamping in the nonlinear range. This level of damping is similar to other studies (*e.g.,* van

de Lindt et al. 2010; Pang and Shirazi 2013); adding more damping would reduce the drifts and damage somewhat, but more work is needed to verify if this would be appropriate.

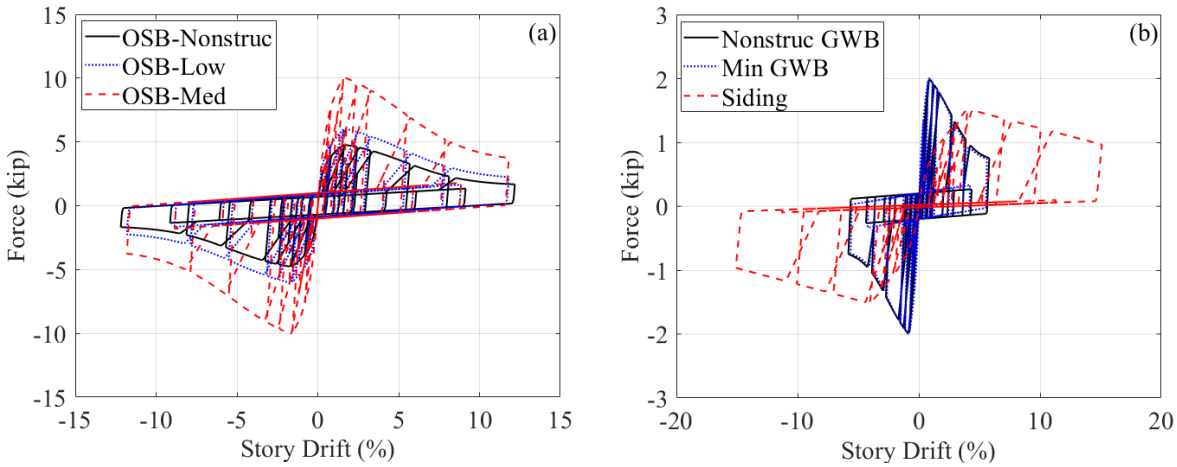

Figure 7. Hysteretic properties for 8 ft (2.4 m) by 10 ft (3 m) wall components showing (a) the OSB components, and (b) the GWB components and the exterior siding.

For model verification, we ran pushover and eigenvalue analyses as reported in Table 1 and Figure 8. The fundamental periods are consistent with expectations for central U.S. construction. The east-west direction is slightly stiffer and has more overstrength than the north-west direction for all buildings because of the architectural configurations. All of the buildings' ultimate strengths are substantially higher than the required design values, due to the contribution of nonstructural walls and finishes to the overall strength of the models.

Table 1. Fundamental periods of buildings.

	Multi-Family	Commercial	Single-Family
Fundamental Period in the N-S direction, T_{NS} (s)	0.48	0.56	0.34
Fundamental Period in the E-W direction, T_{EW} (s)	0.47	0.47	0.31

DAMAGE IDENTIFICATION

We use fragility curves for damage to light-frame wood shear walls from FEMA P-58 (FEMA 2012) to identify damage in buildings. These fragility curves represent the conditional probability of reaching or exceeding a damage state of interest, conditioned on the engineering demands. For the components of interest, the relevant demand parameter is story drift ratio

(SDR). SDR is the largest drift observed in the building for a given ground motion in either story in either direction. FEMA P-58 provides fragilities for a number of different wood shear wall components (FEMA 2012). Each component has multiple damage states, ranging from least, defined in FEMA P-58 as damage state 1, to most severe. As our goal is to identify a damage threshold (DT) corresponding to the onset or earliest occurrence of damage, the damage state of interest is damage state 1.

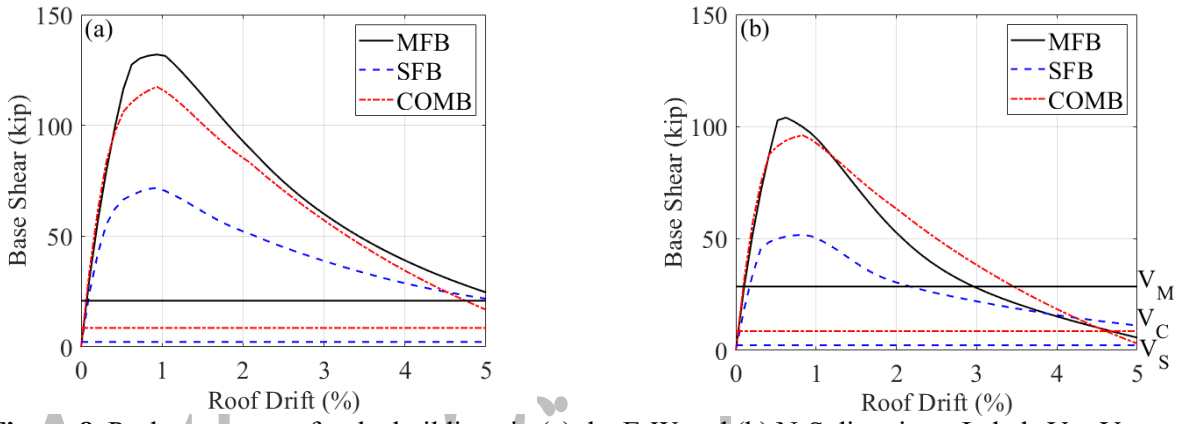

Figure 8. Pushover curves for the buildings in (a) the E-W and (b) N-S directions. Labels V_M, V_C, and V_S in (b) indicate the design base shear for the multi-family, commercial, and single-family buildings, respectively.

Our primary DT of interest corresponds to nail separation from sheathing, screws popping out, and minor cracking of gypsum wallboard, which is primarily cosmetic damage to a very common component of wood frame buildings, but damage that most homeowners would choose to repair. We refer to this DT as $\mathbf{DT_B}$, and it occurs at a median SDR of 0.21% (with a logarithmic standard deviation or σ_{ln} of 0.6) , as shown in Figure 9 (based on FEMA 2012 for NISTIR Classification B1071.041). We also consider two other DT to represent the onset of different kinds of damage. $\mathbf{DT_A}$ represents damage to less well constructed systems, or damage to walls with stucco, and is defined with a median SDR of 0.17%. (This DT could be refined if FEMA P-58 had more data for typical central U.S. cladding materials, which may be more vulnerable.) $\mathbf{DT_C}$ represents more severe damage (*e.g.,* cracking or crushing of wall boards; buckling of studs, etc.); for $\mathbf{DT_C}$ we use a median SDR of 1%. To account for uncertainties in

the drift demands and the DT thresholds, we employ a simple Monte Carlo simulation that randomly generates demands (based on the distribution from structural analysis simulations) and capacity (based on the defined fragility curve). This process is repeated 250 times, such that the probability of damage is the number of realizations in which the randomized demand exceeded the randomized damage threshold, divided by 250; 250 realizations were found to provide good stability in probability results.

Alternative Damage Identification Method

From the 1930 to the 1980s, the United States Bureau of Mines (USBM) studied various aspects of ground vibrations produced by mine blasting frequencies with the goal of engineering surface mining blasts to avoid adverse effects on residential buildings. The USBM studies define the damage threshold as: “loosening of paint; small plaster cracks between construction elements; [and] lengthening of old cracks” (Siskind et al. 1981). One major study was Bulletin 656 (Nicholls et al. 1942), which used peak ground velocity (PGV) to define damage thresholds for single-family residential type structures, defining a damage threshold in terms of a PGV of 2 in/s (5.1 cm/s). Subsequent studies, namely USBM Report 8507 (Siskind et al. 1981), suggested that the blanket damage threshold be modified to account for the dominant frequency content of the blast, which was observed to impact damage in residential type structures. These thresholds were based on measurements of ground-vibration induced damage in 76 single-family residential homes from 219 production blasts, which were combined with nine other blasting studies. The study concluded that, for blasts with dominant frequency of less than 40 Hz (periods greater than 0.025 s), a threshold of 0.75 in/s (1.9 cm/s) is appropriate, while for blasts with dominant frequencies greater than 40 Hz (periods less than 0.025 s), the threshold should remain at 2 in/s (5.1 cm/s).

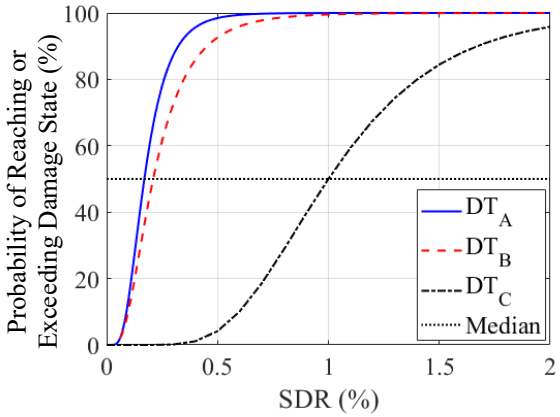

Figure 9. Fragility curves used to define $\mathbf{DT_A}$, $\mathbf{DT_B}$, and $\mathbf{DT_C}$. Each DT represents different types of damage.

To take advantage of the wealth of field data generated in the USBM studies, we adopt here the PGV threshold of 2 in/s (5.1 cm/s) as an alternative damage threshold. We compared the PGV of each ground motion to the threshold PGV to determine if the single-family building was damaged; we chose the single-family building because it is most similar to the buildings used in the USBM studies. Although induced earthquakes generally have dominant frequencies less than 40 Hz (periods greater than 0.025 s), we adopt the larger 2.1 in/s threshold. We make this decision because the buildings Siskind et al. (1981) assigned to the lower damage threshold of 0.75 in/s (1.9 cm/s) were older and especially susceptible to cracking because they had plaster finishes on interior walls. For the modern buildings of interest here with drywall, we judged this lower limit to be excessively pessimistic.

RESULTS

DAMAGE PROBABILITIES FOR THE MULTIFAMILY BUILDING

Drift Demands in Earthquake Scenarios

We first examine trends in drift demands in the multi-family building in the Earthquake Scenarios in Figure 10, as drift demands are the primary input to the damage threshold assessment. For this building, the peak SDR always occurs in the first story and in the weaker/less stiff North-South direction. SDRs in this building increase as the Earthquake

Scenario magnitude increases and as the earthquake occurs closer to the building, which is to be expected. For this structure inelastic response begins around 0.2-0.4% drift. There is an order of magnitude increase in drifts between the Scenarios with **M** 4 and **M** 5.

In Figure 10, it appears that the variability in the drifts may increase as the earthquake becomes closer to the structure and as its magnitude increases. However, the standard deviation in log space of the SDRs is relatively constant across Scenarios, with a mean value of 0.65 (this calculation removes any drifts for buildings that collapsed). We selected ground motions to match the target spectrum in terms of both mean and variability; as a result, we observe record-to-record variability even when the structure is responding in the linear range.

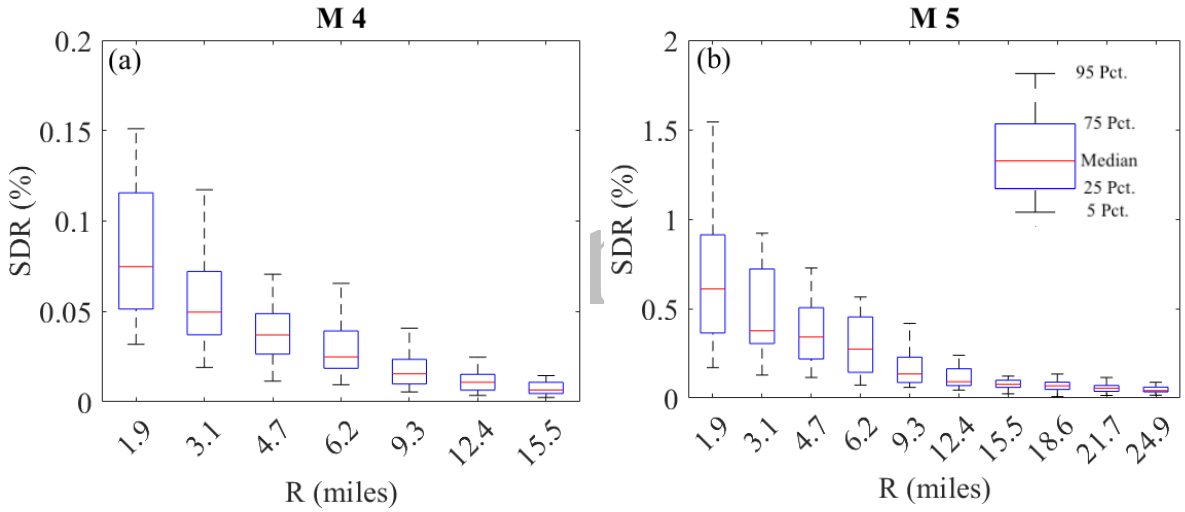

Figure 10. Drift demands in the multi-family building from Earthquake Scenarios with (a) **M** 4 and (b) **M** 5.

In some of the ground motions, the multi-family building collapsed. Collapse is defined as SDR > 10% (Chase 2018). Collapse occurred in less than 1% of all the ground motions run, as would be expected based on observed damage in the region from past events, and was more likely in the more intense very close distance scenarios (reported in Figure 11).

Damage Threshold Probabilities

As expected, as the earthquake magnitude becomes larger and the event occurs closer to the building, the probabilities of exceeding the damage thresholds increase. The probability of

damage is less than 10% for all Scenarios until reaching **M** 4.0 at **R** of 1.9 miles (3 km); the more intense Scenarios have damage probabilities exceeding 10% (Figure 11).

We define the distance laterally (*i.e.,* in map view or epicentral distance) between the earthquake and the building at which the probability of damage reaches 50%, $\mathbf{E_{50}}$, as a measure of the footprint of the Earthquake Scenario's damage for a given building. These values are determined through linear interpolation from the available results. We also consider an alternative metric, $\mathbf{E_{15}}$, which describes the epicentral distance associated with a 15% probability of damage. We chose 15% as a more conservative damage identifier that may be of interest to some decision makers. Figure 12 reports and compares the $\mathbf{E_{15}}$ and $\mathbf{E_{50}}$ values for different magnitude events. For **M** < 4.5, neither 15% nor 50% probability of damage are reached for any epicentral distances. The larger earthquakes can cause damage over a radius of 20 to 80 miles, depending on which metric is used.

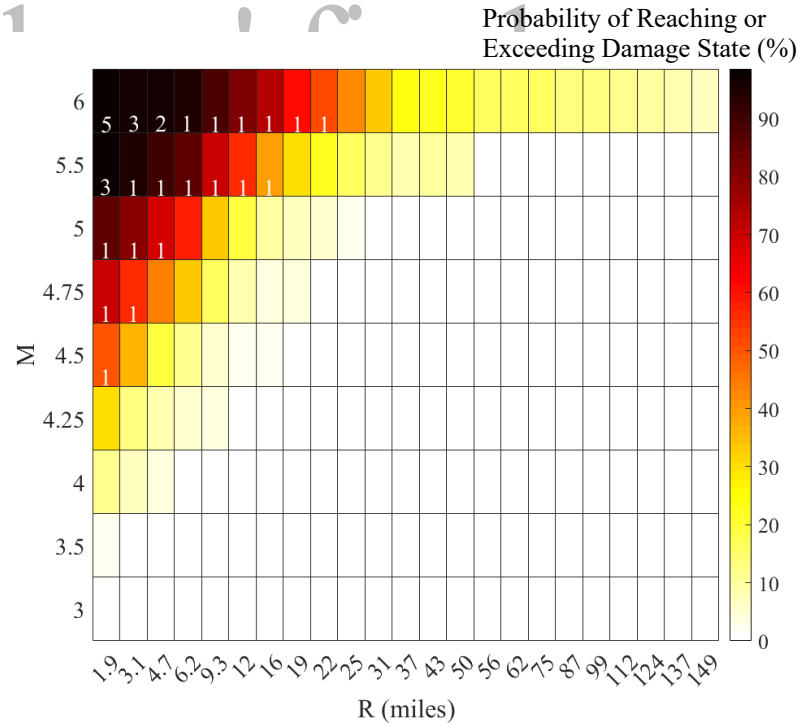

Figure 11. Probability of damage for the multi-family building for all Earthquake Scenarios, based on $\mathbf{DT_B}$. The white numbers represent the instances of collapse out of the 25 ground motions for that Scenario.

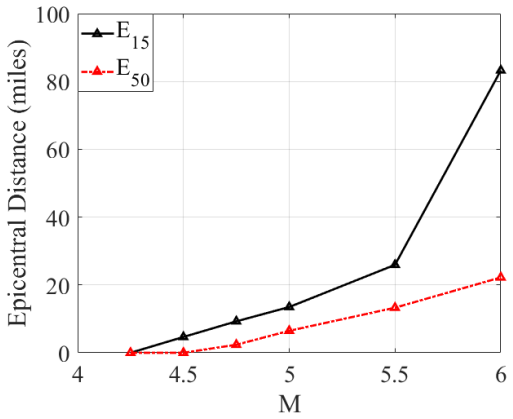

Figure 12. Spatial footprint of damage quantified in terms of $\mathbf{E_{15}}$ and $\mathbf{E_{50}}$ for the multi-family building, based on $\mathbf{DT_B}$.

DAMAGE PROBABILTIES FOR OTHER BUILDINGS

As shown in Figure 13, the median commercial building drifts are on average 10% larger than the multi-family building, for a given Earthquake Scenario. The commercial building has a longer period (T_{NS} = 0.56 s) as a result of fewer shear walls compared to the multi-family building and a larger seismic weight. The single-family building has the shortest period (T_{NS} = 0.34 s) considered in this study, and has the lowest seismic weight (i.e. smallest seismic inertial demands) and, thus, the lowest drifts. For all the buildings, the largest drift tends to occur in the first story in the North-South direction. As a result of the associated drift demands on the buildings, Figure 14 shows that the single-family building has the lowest probability of damage for all Earthquake Scenarios, and the commercial-family building has the highest. These differences in the probability of damage are typically less than 10%.

We compare the spatial footprints of damage for the three buildings. The spatial footprint metric, $\mathbf{E_{50}}$, for earthquakes $\mathbf{M} < 5$ is similar for the three building types, as plotted in Figure 15. Note that an $\mathbf{E_{15}}$ or $\mathbf{E_{50}}$ value of 0 may still imply that the building exceeds the selected damage percentile if located immediately above the earthquake (*i.e.,* earthquake depth = hypocentral distance). For **M** 5.5 and **M** 6.0, it becomes clear that the weaker buildings are

likely to be damaged at further distances away because of greater drift demands and nonlinear response appearing in less intense Earthquake Scenarios.

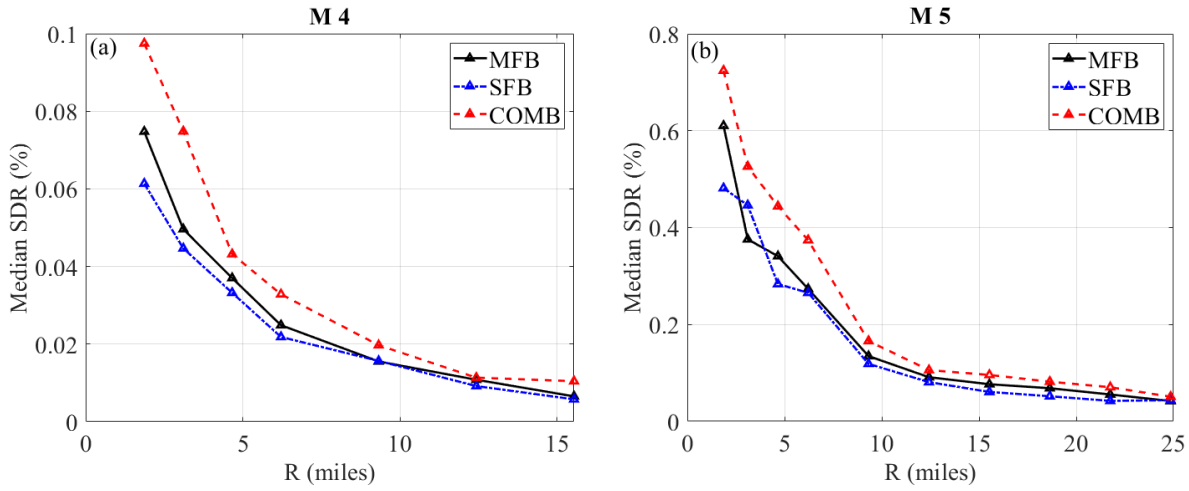

Figure 13. Comparison of drift demands in the multi-family (MFB), commercial (COMB) and single-family (SFB) buildings from Earthquake Scenarios with (a) **M** 4 and (b) **M** 5.

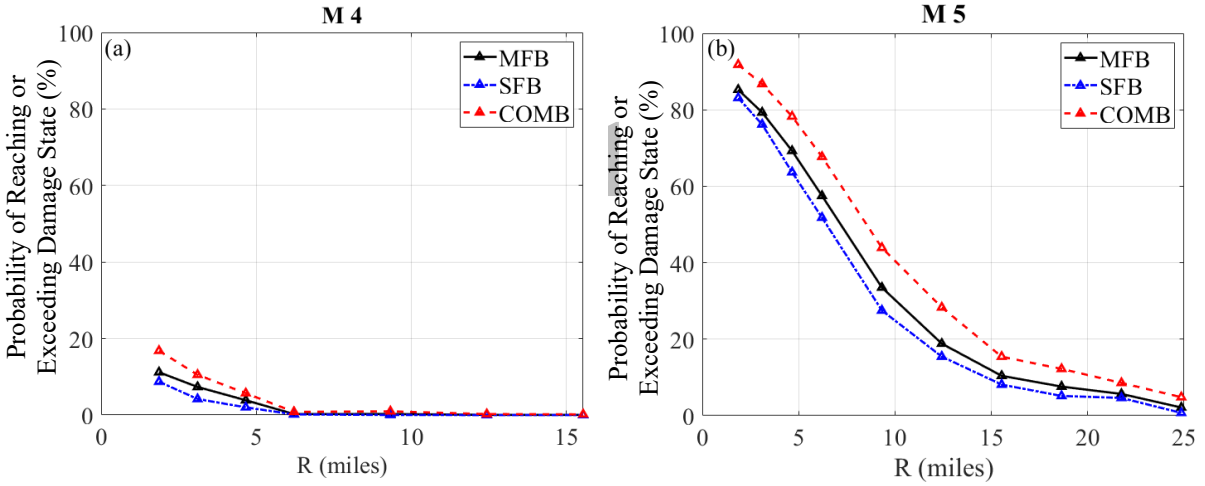

Figure 14. Comparison of damage probabilities in the multi-family (MFB), commercial (COMB) and single-family (SFB) buildings from Earthquake Scenarios with (a) **M** 4 and (b) **M** 5.

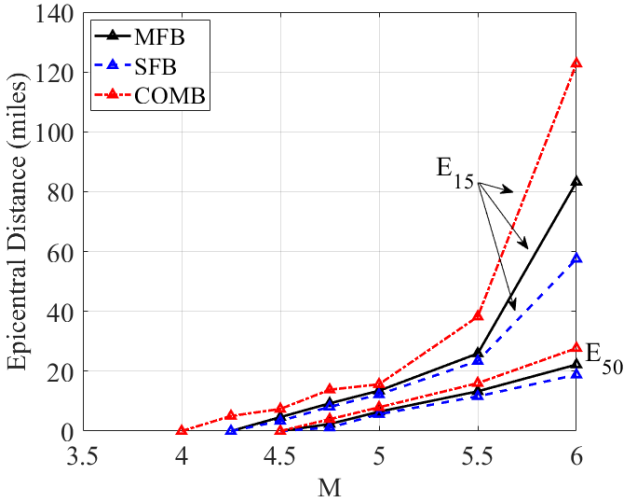

Figure 15. Spatial footprint of damage quantified in terms of $\mathbf{E_{15}}$ and $\mathbf{E_{50}}$ for in the multi-family (MFB), commercial (COMB) and single-family (SFB) buildings, based on $\mathbf{DT_B}$.

DAMAGE PROBABILTIIES FOR OTHER THRESHOLD DEFINITIONS

The impact of the three different DT on damage probabilities for the multi-family buildings is investigated in Figure 16. Results for $\mathbf{DT_A}$ and $\mathbf{DT_B}$ are similar due to very similar median thresholds. $\mathbf{DT_C}$ indicates more serious damage. The implications of these thresholds for the spatial footprint of the damage are illustrated in Figure 17. To be expected, the lowest considered damage threshold ($\mathbf{DT_A}$) has the largest spatial extent. These results show that, if one is concerned with only the more severe damage represented by $\mathbf{DT_C}$, the spatial footprints are much more limited (<15 miles).

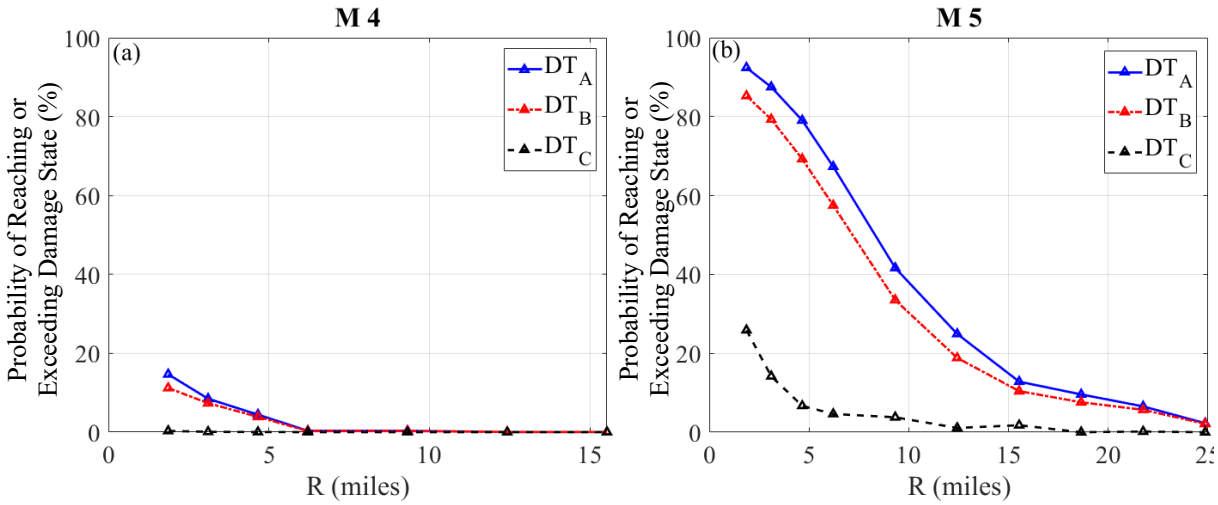

Figure 16. Damage probabilities based $\mathbf{DT_A}$, $\mathbf{DT_B}$, and $\mathbf{DT_C}$ for the multi-family building for (a) **M** 4 and (b) **M** 5.

Figure 18 compares our FEMA P-58-based damage thresholds to the USBM damage threshold of 2 in/s (5.1 cm/s) PGV for the single-family building (the closest comparison to the USBM data). That threshold seems to indicate that the older buildings that were the basis for the USBM threshold are more vulnerable to damage, producing much larger spatial footprints of damage.

DISCUSSION AND IMPLICATIONS

PERFORMANCE OF THE WOOD LIGHT-FRAME BUILDING STOCK

To examine the implications of these results, we first combine all results into a single plot, representing the average performance of the three light-frame wood buildings examined. Figure 19, for example, reports the average probability of damage across all considered building types in all of the Earthquake Scenarios for $\mathbf{DT_B}$.

Of course, this study only looks at newly constructed (*i.e.,* modern) light-frame wood buildings with residential occupancies. Older buildings likely perform worse, as indicated by the USBM threshold results in Figure 18, as they may be weaker, less stiff, more irregular and have worse quality nailing, connections and/or finishes, making the onset of damage likely earlier (Christovasilis et al. 2009). As a consequence, these results underestimate the potential for induced earthquakes to damage the older and more vulnerable buildings in the Oklahoma building stock. Conversely, this analysis likely overestimates damage to other types of construction, especially hospital and schools, which are designed with "importance factors" that amplify building strength. However, more work would be needed to quantify how much this additional strength protects against onset of damage, and to examine other building types more commonly used for hospitals and critical facilities.

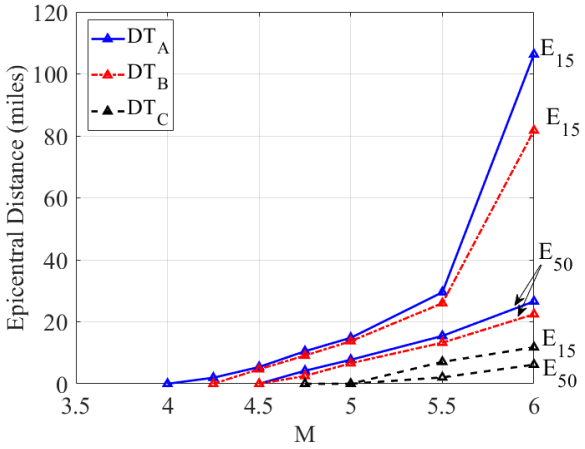

Figure 17. Spatial footprint of damage quantified in terms of E_{15} and E_{50} for the multi-family building, based on $\mathbf{DT_A}$, $\mathbf{DT_B}$, and $\mathbf{DT_C}$.

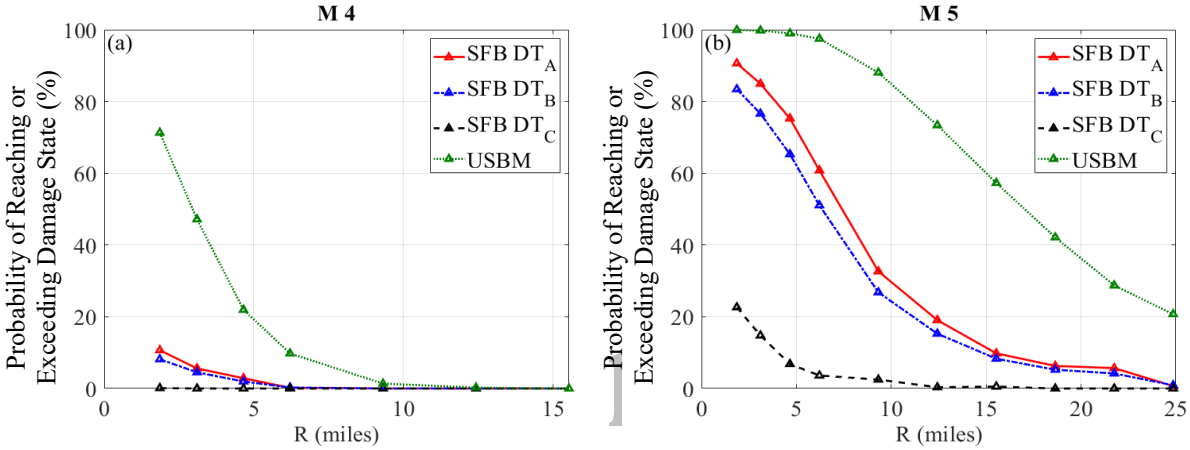

Figure 18. Comparison of damage probabilities for the single-family building for $\mathbf{DT_A}$, $\mathbf{DT_B}$, and $\mathbf{DT_C}$, compared to USBM damage threshold PGV of 2 in/s (5.1 cm/s) for: (a) **M** 4 and (b) **M** 5.

IMPLICATIONS FOR POLICY MAKING

Exposure reduction presents one of the most practical solutions to mitigate the risk of induced seismicity in OK. One possible approach would be to define exclusion zones or setbacks, where new injection operations could not be drilled around critical buildings and infrastructure.

The implications of these results for exclusion zones are explored in Figure 20. This plot shows the location of a well, and the locations of possible earthquakes around that well, recognizing that earthquakes may occur at some distance from the injection. Figure 20a illustrates a case where earthquakes can occur as many as 12 miles (20 km) (laterally; in map view) from the well, based on an upper bound distance observed by Yeck et al. (2016) for the

high-volume wells near Prague, OK. In Figure 20b, the earthquakes are assumed to be within 3 miles (5 km) of the well (Goebel and Brodsky 2018). We then show the spatial extent of damage from different magnitude events based on the $\mathbf{E_{50}}$ metric around the assumed earthquake locations for the "average" building, and two damage thresholds.

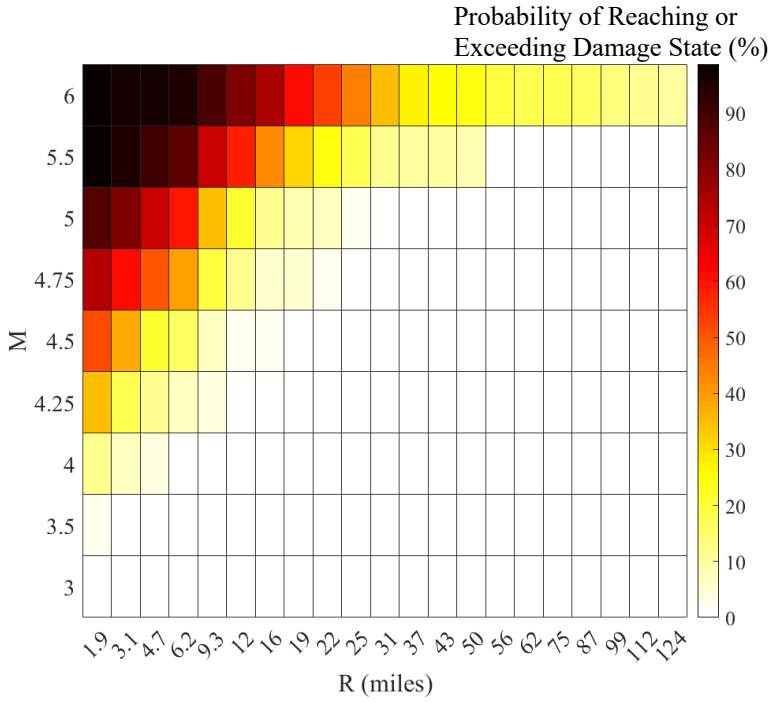

Figure 19. Average probability of damage to modern light-frame wood buildings examined in this study, based on $\mathbf{DT_B}$.

The result for these buildings suggest that exclusion zones or setbacks on the order of 15 to 25 miles may make sense to reduce the risk of damage. These distances are based on **M** 5.5 event, which is on the upper end of the event magnitudes that have been observed, though not the largest possible (Shumway 2019). If we are concerned only with more severe damage represented by $\mathbf{DT_C}$, a zone of 6 to 10 miles may be more appropriate.

These possible setbacks are generally larger than other proposed distances, such as the ~ 6 mi (10 km) value suggested by Atkinson (2017). Parts of Oklahoma are relatively sparsely populated, with 2.5 homes per square mile (U.S. Census Bureau 2007). Despite this relatively low density of construction in some areas of Oklahoma, it is likely impractical to site wells this far from all buildings/infrastructure. However, it may be possible to maintain this distance from

critical facilities, such as hospitals, and denser housing areas. These zones have the potential to greatly reduce damage to the built environment. Figure 20 and the underlying results, can also inform post-earthquake damage inspections, implying, for example, inspection radii for bridges and other structures that may require evaluation after potentially damaging events (Harvey et al. 2018).

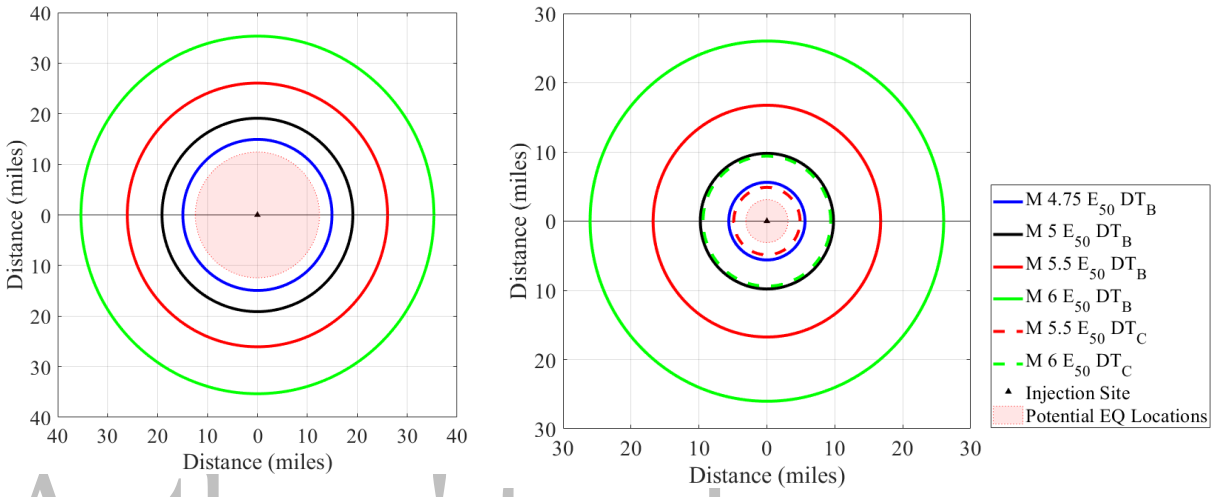

Figure 20. Spatial footprint of damage from an injection site in (a) assuming an earthquake may occur up to 12 miles from the well for $\mathbf{DT_B}$, and (b) assuming an earthquake occurs up to 3 miles from the well for $\mathbf{DT_B}$ and $\mathbf{DT_C}$.

In terms of magnitude thresholds, these results show that **M** < 4 events would very rarely cause damage to the light-frame wood buildings that make up the majority of our residential housing infrastructure. Even a **M** 4.5 event causes fairly limited damage (with minor damage to less than 15% of buildings of this type beyond about 6 miles from the earthquake). Recall that magnitude thresholds are commonly used as part of Traffic Light Systems to regulate well operations with the goal of reducing seismic hazard. Our findings confirm that the magnitude thresholds being used (*e.g.,* **M** 1 in Ohio) are well below those associated with the onset of damage. Moreover, the results suggest that seismic hazard reduction policies that aim to reduce the likelihood of **M** > 4 events would likely be effective at preventing most damage from induced events. However, the findings here do not imply that a red-light threshold of **M** 4

513 would be acceptable, or adequately reduce the risk of future earthquakes, for which a lower
514 threshold would likely be desirable (*e.g.,* Green et al. 2012).

515 It is well known, of course, that **M** alone is not a good predictor of structural damage (due
516 to impacts of fault mechanism, soil conditions, etc.). Therefore, there is interest in Traffic Light
517 thresholds based on observed ground shaking rather than **M** alone (*e.g.,* Bommer et al. 2015;
518 Majer et al. 2012; Wong et al. 2015). We quantify ground shaking in terms of PGV because it
519 has been correlated with structural damage in small to moderate magnitude events in previous
520 studies, *e.g.,* Siskind et al. 1981. Our results, taken for all the Scenarios together, suggest that
521 the PGV corresponding to 15% chance of damage for modern buildings is approximately 7 in
522 /s (12 cm/s); the median PGV associated with damage is about 12 in/s (30 cm/s). These
523 thresholds would be associated with damage in the identified percentage of modern light wood-
524 frame buildings. Older buildings would be damaged at lower PGV thresholds.

525 **CONCLUSIONS**

526 This study examines the potential for damage to modern wood light-frame buildings in
527 Oklahoma due to induced earthquakes of varying magnitude. The simulations are based on two-
528 story commercial, multifamily, and single-family buildings, which are designed with lateral
529 strength and detailing consistent with modern code requirements in Pawnee, OK, and modeled
530 nonlinearly in the Timber3D software. Ground shaking for each Earthquake Scenario is defined
531 by target spectra from an Oklahoma-based ground motion prediction equation. For each
532 scenario, 25 records are selected to match the target spectra, providing the excitation for the
533 simulation models. Damage is identified as occurring if story drifts exceed a level associated
534 with screws or nails popping out, minor cracking of wallboard, and warping or cracking of
535 wallpaper in light-frame wood shear walls. This damage is mostly minor and mostly cosmetic,
536 but many homeowners would choose to repair it.

The results show that earthquakes with magnitudes less than 4 or 4.25 cause very limited damage to these kinds of buildings. For larger magnitude events, the distance between the epicenter and buildings that are potentially damaged ranges from 3 miles for a magnitude 4.75 event, to 22 miles for a magnitude 6; the extent of damage beyond an injection well is larger because earthquakes may occur some distance from the associated well(s). If we are concerned only with more severe damage, the footprint over which the damage occurs is smaller*, i.e.,* about 8 miles measured from the epicenter in the case of a magnitude 6 event. The simulations show that the single-family building is least damaged, and the commercial building most damaged of the buildings considered, but these differences are small, typically changing damage probabilities by less than 10%. These results, however, are based on a subset of analyzed structures all of the light-frame wood type, and we expect that masonry buildings and older wood frame buildings would be more vulnerable (*i.e.,* damageable at lower magnitudes, and damage extending over larger footprints). Critical facilities, such as hospitals, are likely less damageable. The effects of soil conditions and soil-structure-interaction were not considered, nor were near fault spectral shape effects.

The anthropogenic earthquakes occurring in the region around Oklahoma raise new questions about the types of damage that can be caused by small to moderate magnitude events, and effective strategies for mitigating the risks of that damage. This study indicates that earthquakes with magnitudes greater than 4.5 are likely to be associated with damage to buildings, with expanding footprints of damage for larger magnitude events. Exclusion zones on the order of tens of miles may be appropriate between high volume injection wells capable of producing earthquakes and critical infrastructure.

ACKNOWLEDGMENTS

This material is supported by the National Science Foundation under Grant No. 1515438 to the Colorado Collaboratory for Induced Seismicity. The authors acknowledge the help of Zach

Bullock, Eric Johnson and Jakub Valigura in preparing the manuscript. We thank Ershad Ziaei Ghehnavieh and Weichiang Pang for sharing their models of wood light frame buildings (from the ATC 116 project), which were modified for Pawnee, OK in this study. This work utilized the RMACC Summit supercomputer, which is supported by the National Science Foundation, the University of Colorado Boulder, and Colorado State University. Conversations with Gail Atkinson motivated the idea for this study. We appreciate the valuable feedback provided by three anonymous reviewers.

REFERENCES

ASCE. (2017). *ASCE/SEI 7-16: Minimum Design Loads and Associated Criteria for Buildings and Other Structures*. ASCE/SEI, Reston, VA.

American Society of Civil Engineers (ASCE). (2011). 7-10: *Minimum Design Loads for Buildings and Other Structures.* ASCE/SEI, Reston, VA.

Assatourians, K., and Atkinson, G. M. (2018). "Processed ground-motion records for induced earthquakes for use in engineering applications." Personal Communication.

ATC. (2019). "Active Projects." *ATC*, <https://www.atcouncil.org/projects/projects-active> (Feb. 1, 2019).

Atkinson, G., Wald, D., Worden, C., & Quitoriano, V. (2018). The Intensity Signature of Induced Seismicity. *Bulletin of the Seismological Society of America, 108*(3A), 1080-1086.

Atkinson, G. M. (2017). "Strategies to prevent damage to critical infrastructure due to induced seismicity." FACETS, 2(1), 374–394.

Authentic Custom Homes. (2018) Homes by Taber LLC, Silver Custom Homes and Sun Custom Homes. Typical siding in Oklahoma, Oklahoma.

Baird, B.W. (2019). " Quantifying the Onset of Damage for Light Frame Wood Buildings in Induced Earthquakes". M.S. Thesis. University of Colorado Boulder.

Baker, J. W., and Lee, C. (2018). "An Improved Algorithm for Selecting Ground Motions to Match a Conditional Spectrum." *Journal of Earthquake Engineering*, 22(4), 708–723.

Barba-Sevilla, M., Baird, B., Liel, A., and Tiampo, K. (2018). "Hazard Implications of the 2016 Mw 5.0 Cushing, OK Earthquake from a Joint Analysis of Damage and InSAR Data." *Remote Sensing*, 10(11), 1715.

Department for Business, Energy, and Industrial Strategy (BEIS). (2013). "Managing onshore induced seismicity." GOV.UK available at: <https: //www.gov.uk/government/publications/traffic-lightmonitoring-system-shale-gas-and-fracking>.

Bommer, J. J., Crowley, H., and Pinho, R. (2015). "A risk-mitigation approach to the management of induced seismicity." *Journal of Seismology*, 19(2), 623–646.

Brown, M.R.M., Ge, S., Sheehan,A.F., and Nakai, J.S. (2017). "Evaluating the effectiveness of seismicity mitigation: numerical modeling of wastewater injection near Greeley, Colorado." *Journal of Geophysical Research: Solid Earth*, 122, 6569–6582.

Chase, R., Liel, A.B., Luco, N., Baird, B., "Seismic Loss and Damage in Light-Frame Wood Buildings from Sequences of Induced Earthquakes". *Earthquake Engineering and Structural Dynamics,* In Press.

Chase, R. E. (2018). "Structural Response and Risk Considering Regional Ground Motion Characteristics." PhD Thesis, University of Colorado at Boulder.

Christovasilis, I. P., Filiatrault, A., Constantinou, M. C., and Wanitkorkul, A. (2009). "Incremental dynamic analysis of woodframe buildings." *Earthquake Engineering & Structural Dynamics*, 38(4), 477–496.

Clayton, P., Zalachoris, G., Rathje, E., Bheemasetti, T., Caballero, S., Yu, X., and Bennett, S. (2016). "The Geotechnical Aspects of the September 3, 2016 M5.8 Pawnee, Oklahoma Earthquake." *GEER Reconnasissance Team Report.* Available at: http://learningfromearthquakes.org/2016-09-03-oklahoma/images/2016_09_03_oklahoma/pdfs/Pawnee-GEERreport-FINAL_v1.2.pdf

COGCC (2017). 2017 Annual Report. Available at: https://cogcc.state.co.us/documents/library/Technical/WQCC_WQCD%20Annual%20Reports/2017%20ANNUAL% 20REPORT%20WQCC_FINAL_12302017.pdf

Ellsworth, W. L., Llenos, A. L., McGarr, A. F., Michael, A. J., Rubinstein, J. L., Mueller, C. S., Petersen, M. D., and Calais, E. (2015). "Increasing seismicity in the U. S. midcontinent: Implications for earthquake hazard." *The Leading Edge*, 34(6), 618–626.

FEMA. (2012). "Seismic Performance Assessment of Buildings." P-58-1, 278.

Folz, B., and Filiatrault, A. (2001). "Cyclic Analysis of Wood Shear Walls." *Journal of Structural Engineering*, 127(4), 433–441.

Frohlich, C., DeShon, H., Stump, B., Hayward, C., Hornbach, M., and Walter, J. I. (2016). "A Historical Review of Induced Earthquakes in Texas." *Seismological Research Letters*, 87(4), 1022–1038.

Goebel, T. H. W., and Brodsky, E. E. (2018). "The spatial footprint of injection wells in a global compilation of induced earthquake sequences." *Science*, 361(6405), 899–904.

Green, C.A., P. Styles, B.J. Baptie (2012). "Preese Hall shale gas fracturing: review and recommendations for induced seismic mitigation." Report to DECC, available at: https://www.gov.uk/government/uploads/system/uploads/attachment_data/file/48330/5055-preese-hall-shale-gasfracturing-review-and-recomm.pdf

Ground Water Protection Council (GWPC) and Interstate Oil and Gas Compact Commission (IOGCC). (2017). *Potential Injection-Induced Seismicity Associated with Oil & Gas Development: A Primer on Technical and Regulatory Considerations Informing Risk Management and Mitigation.*

Harvey, P.S., Henrich, S.K., and Muraleetharan, K.J. (2018). "A Framework for Post-Earthquake Response Planning in Emering Seismic Regions." *Earthquake Spectra*, 34(2), 503-525.

Langenbruch, C., Weingarten, M., and Zoback. M.D. (2018). "Physics-based forecasting of man-made earthquake hazards in Oklahoma and Kansas." *Nature Communications* 9, 3946.

Langenbruch, C., and Zoback, M.D. (2016). " How will induced seismicity in Oklahoma respond to decreased saltwater injection rates?" *Science Advances*.

Lin, T., Haselton, C. B., and Baker, J. W. (2013). "Conditional spectrum-based ground motion selection. Part I: Hazard consistency for risk-based assessments: Conditional spectrum-based ground motion selection." *Earthquake Engineering & Structural Dynamics*, 42(12), 1847–1865.

Liu, T. J., Luco, N., and Liel, A. B. (2019). "Increases in Life-Safety Risks to Building Occupants from Induced Earthquakes in the Central United States." *Earthquake Spectra*, 35(2), 471-488.
Majer, E., Nelson, J., Robertson-Tait, A., Savy, J., and Wong, I. (2012). *Protocol for Addressing Induced Seismicity Associated with Enhanced Geothermal Systems* DOE/EE-0662.
Moschetti, M., Thompson, E., Powers, P., Hoover, S., & McNamara, D. (2019). Ground Motions from Induced Earthquakes in Oklahoma and Kansas. *Seismological Research Letters*, 90(1), 160-171
Mutz, K. (2019) Comparison of State and Federal Regulations to Manage Induced Seismicity from Class II Injection Wells, *The Policy Surveillance Program, a Law Atlas Project of the Public Health Law Research Program*, http://LawAtlas.org/seismicity.php (coming soon)
Nicholls, H. R., Johnson, C. F., and Duvall, W. I. (1942). *Blasting Vibrations and their Effects on Structures.* US Department of Interior Bureau of Mines, 110.
Novakovic, M., Atkinson, G. M., and Assatourians, K. (2018). "Empirically Calibrated Ground-Motion Prediction Equation for Oklahoma." *Bulletin of the Seismological Society of America*, 108(5A), 2444–2461.
Oklahoma Geologic Survey (OGS). (2018). "Oklahoma Earthquakes Magnitude 3.0 and greater." Available at: https://earthquake.usgs.gov/earthquakes/byregion/oklahoma/OK-M3-dec3-2018.pdf
Pang, W., and Shirazi, S. M. (2013). "Corotational Model for Cyclic Analysis of Light-Frame Wood Shear Walls and Diaphragms." *Journal of Structural Engineering*, 139(8), 1303–1317.
Petersen, M. D., Mueller, C. S., Moschetti, M. P., Hoover, S. M., Llenos, A. L., Ellsworth, W. L., Michael, A. J., Rubinstein, J. L., McGarr, A. F., and Rukstales, K. S. (2016). *2016 One-Year Seismic Hazard Forecast for the Central and Eastern United States from Induced and Natural Earthquakes*. Open-File Report, U.S. Geological Survey.
Petersen, M. D., Mueller, C. S., Moschetti, M. P., Hoover, S. M., Rukstales, K. S., McNamara, D. E., Williams, R. A., Shumway, A. M., Powers, P. M., Earle, P. S., Llenos, A. L., Michael, A. J., Rubinstein, J. L., Norbeck, J. H., and Cochran, E. S. (2018). "2018 One-Year Seismic Hazard Forecast for the Central and Eastern United States from Induced and Natural Earthquakes." *Seismological Research Letters*, 89(3), 1049–1061.
Petersen, M. D., Mueller, C. S., Moschetti, M. P., Hoover, S. M., Shumway, A. M., McNamara, D. E., Williams, R. A., Llenos, A. L., Ellsworth, W. L., Michael, A. J., Rubinstein, J. L., McGarr, A. F., and Rukstales, K. S. (2017). "2017 One-Year Seismic-Hazard Forecast for the Central and Eastern United States from Induced and Natural Earthquakes." *Seismological Research Letters*, 88(3), 772–783.
Rubinstein, J. L., and Mahani, A. B. (2015). "Myths and Facts on Wastewater Injection, Hydraulic Fracturing, Enhanced Oil Recovery, and Induced Seismicity." *Seismological Research Letters*, 86(4), 1060–1067.
Shumway, A. (2019). Personal communication: Deaggregation of USGS One-year forecast for Pawnee.
Siskind, D. E., Stagg, M. S., Kopp, J. W., and Dowding, C. H. (1981). *Structure response and damage produced by ground vibration from surface mine blasting*. US Bureau of Mines.
Taylor, J., Çelebi, M., Greer, A., Jampole, E., Masroor, A., Melton, S., Norton, D., Paul, N., Wilson, E., and Xiao, Y. (2016). "M5.0 Cushing, Oklahoma, USA Earthquake on

November 7, 2016." *EERI Earthquake Reconnaisance Team Report.* Available at : http://learningfromearthquakes.org/2016-09-03-oklahoma/images/2016_09_03_oklahoma/pdfs/Oklahoma-EERI-Recon-Report-2017-02-15-Finalized.pdf

U.S. Census Bureau. (2007). "Oklahoma Census Data: Population & Housing Density." <https://www.census-charts.com/Density/Oklahoma.html> (Feb. 1, 2019).

van de Lindt, J. W., Pei, S., Liu, H., and Filiatrault, A. (2010). "Three-Dimensional Seismic Response of a Full-Scale Light-Frame Wood Building: Numerical Study." *Journal of Structural Engineering*, 136(1), 56–65.

van Elk, J., Bourne, S., Oates, S.J., Bommer, J.J., Pinho, R., and Crowley, H. (2019). "A probabilistic model to evaluate options for mitigating induced seismic risk." *Earthquake Spectra*, 35(2), 481-498.

Walters, R. J., Zoback, M. D., Baker, J. W., and Beroza, G. C. (2015). "Characterizing and Responding to Seismic Risk Associated with Earthquakes Potentially Triggered by Fluid Disposal and Hydraulic Fracturing." *Seismological Research Letters, 8*6(4), 1110–1118.

Weingarten, M., Ge, S., Godt, J. W., Bekins, B. A., and Rubinstein, J. L. (2015). "High-rate injection is associated with the increase in U.S. mid-continent seismicity." *Science*, 348(6241), 1336–1340.

Wong, I., Nemser, E., Bott, J., and Dober, M. (2015). *Induced Seismicity and Traffic Light Systems as Related to Hydraulic Fracturing in Ohio*. Report to Ohio Oil and Gas Association, Columbus, Ohio.

Yeck, W. L., Weingarten, M., Benz, H. M., McNamara, D. E., Bergman, E. A., Herrmann, R. B., Rubinstein, J. L., and Earle, P. S. (2016). "Far-field pressurization likely caused one of the largest injection induced earthquakes by reactivating a large preexisting basement fault structure: Faireview Earthquake on 13 February 2016." *Geophysical Research Letters*, 43(19), 10,198-10.

Yong, A., Thompson, E. M., Wald, D., Knudsen, K. L., Odum, J. K., Stephenson, W. J., and Haefner, S. (2016). "Compilation of Vs30 Data for the United States: U.S. Geological Survey Data Series 978." 8.

Zalachoris, G., and Rathje, E. M. (2019). "Ground Motion Model for Small-to-Moderate Earthquakes in Texas, Oklahoma, and Kansas." *Earthquake Spectra*, 35(1), 1–20.

Ziaei Ghehnavieh, E. Z. (2017). "Seismic Analysis of Light-Frame Wood Buildings with a Soft-Story Deficiency." PhD Thesis, Clemson University.